

The Frank slide (Alberta, Canada): from the contributing factors to the processes of propagation



F.Humair, M. Charrière, A. Pedrazzini, M. Güell i Pons, M.Volpi, L.Foresti, & M.Jaboyedoff
Institute of Geomatics and Risk Analysis, University of Lausanne, Switzerland
 J-L. Epard
Institute of Geology and Paleontology, University of Lausanne, Switzerland
 C. Froese
Alberta Geological Survey, Canada

ABSTRACT

The Frank slide is a rock avalanche that took place in 1903. The aim of this paper is to study the geological features of Turtle Mountain in terms of structural and engineering geology as well as a lithological, granulometrical and morphological description of the deposit. Some modelling (SVR by Matlab) complete the analysis. The results show that part of the fracturing is related to the folding of the anticline and that the hinge area has a large influence on the rock mass quality. The description of the deposit allows making assumptions on the collapse mode.

RÉSUMÉ

En 1903, il s'est produit une avalanche rocheuse connue sous le nom de Frank slide. Cette étude vise à analyser les éléments géologiques qui ont amené à la rupture. De plus, une description granulométrique, lithologique et morphologique du dépôt est réalisée. Des modélisations (SVR par Matlab) complètent l'analyse. Les résultats indiquent que la fracturation est en grande partie en lien avec le plissement de l'anticlinal. De plus, l'influence de la zone charnière du pli sur la qualité du massif rocheux a été démontrée. La description du dépôt permet de proposer un mode d'effondrement.

1 INTRODUCTION

On the night of the 29th of April 1903, the eastern flank of the Turtle Mountain anticline (Alberta, Canada, Figure 1) fell down as a huge rock avalanche known as the Frank slide. 30 millions cubic meters of rock collapsed at a speed of 30m/s and buried the village of Frank, where 70 people died (Couture et al. 1998). The failure was structurally controlled (Jaboyedoff et al. 2009, Cruden and Krahn 1973). As a consequence, a large deposit was formed: the travel distance was up to 3 km and it covered an area of a little more than 3 km². The deposit is inversely graded as the fines are at its bottom and the larger boulders at the top. Its mean thickness is 14 m (Cruden and Hungr 1986).

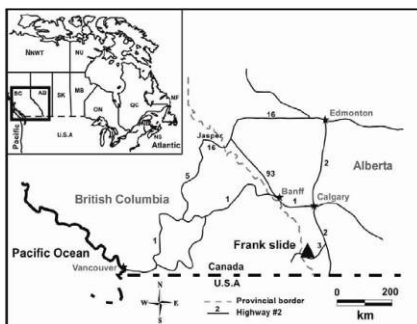


Figure 1. Frank slide's situation map, in Jaboyedoff et al. (2009).

Turtle Mountain is mainly formed by Devonian to Cretaceous limestones (Norris 1993). Figure 2 shows the stratigraphic log.

The majority of outcropping rocks is highly fractured and belongs to the carbonate Livingstone and Mount-Head formations. The deposit is largely composed of Middle Livingstone with small amount of Upper and Lower Livingstone, Mount-Head and Banff formations.

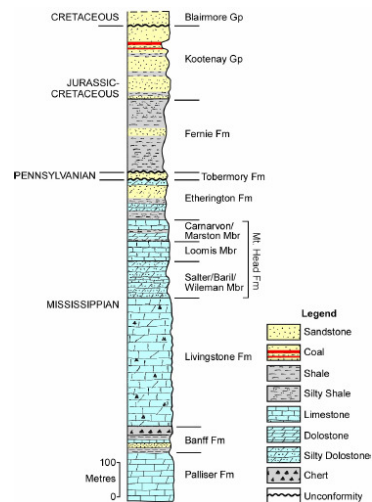


Figure 2. Stratigraphic log of Turtle Mountain area, Langenberg et al. (2007).

This paper is inspired by several previous studies (McConnell and Brock 1903, Cruden and Krahn 1973, Cruden and Hungr 1986, Jones 1993, Benko and Stead 1998, Couture et al. 1996, 1998, Read et al. 2000, Locat et al. 2006, Moreno and Froese 2007, Langenberg et al. 2007, Sturzenegger et al. 2007, Froese et al. 2009a, 2009b, Jaboyedoff et al. 2009, Pedrazzini et al. accepted, Brideau et al. in review.)

More precisely, the present research is conducted to acquire a better understanding of the mechanisms leading to a rock avalanche like Frank slide. It includes the study of all the processes that are taking place from the origin of the contributing factors of the failure to the forms of transportation and deposition. The first consists in a structural geological and geotechnical study in relationship with folding phase and the second in a granulometrical, lithological and morphological description of the deposit.

2 METHODOLOGY

Field surveys were conducted to gather information on Turtle Mountain. Detailed measurements of structural geology and rock mass conditions following ISRM methodology (1977) were carried out. Measurements were taken in several places along and across the fold axis on both sides of the hinge area. Field survey also allowed describing 4786 blocks of the deposit in terms of mean diameter, lithology, geological formation and orientation of the major axis.

Based on the dip-domains technique (Groshong 1999), a cross section of the anticline is constructed to acquire a better understanding its geometry.

The field structural analysis is completed using Coltop 3D software (Jaboyedoff et al. 2007, 2009). Along with geotechnical analysis, Coltop 3D allows defining different structural domains in the mountain which are homogeneous in terms of fracturing and strains. Back cracks identification and displacement of rock's compartments are deduced from fracturing analysis.

Uniaxial Compressive Strength (UCS, measured with the Schmidt hammer), Intact Rock Strength (IRS) and Weathering Grade measurements were carried out following ISRM methodology (1977).

Furthermore, the Geological Strength Index (GSI) (Hoek and Brown 1997, Marinós et al. 2005) is used, in a quantitative approach (Cai et al. 2004) to underline a connection between the distance to the fold axis and the quality of rock mass. It is expected to illustrate the probable influence of the high fracturing density in the hinge area on the weathering of the mountain. This suspected relationship between the distance to the hinge and the GSI can be exploited and integrated into a statistical regression model. Others factors such as elevation (influencing precipitation, wind and the consequent weathering of rock formations), the location in space and the geological structures, are used to build a spatial predictive model of GSI. In this study, the Support Vector Regression (SVR) model is applied to predict GSI from the distance to the hinge, the location in space and

the elevation. SVR is a kernel method for regression estimation (Vapnik 1995). It is particularly adapted to work with high-dimensional and noisy data presenting non-linear relationships. Given a set of training examples $\{(x_i, y_i)\}_{i=1\dots N}$, where x_i is the input vector (distance to hinge, elevation, etc) and y_i is the output (ex: GSI), SVR first maps the data into a higher dimensional space where linear regression $f(x) = w^T x + b$ is possible. Such mapping is computed implicitly by using kernel functions which are measuring the similarity between training measurements. By minimizing a robust error function comprising empirical risk (training error) and model's complexity, SVR provides good generalization abilities on new data.

Remote sensing analysis on the orthophoto (cellsize 0.15 m) was used to provide an automatic evaluation of the granulometry of the deposit's surface. It is based on a morphological operator which can filter brighter or darker elements in order to extract structures (here blocks) from the image. In this case, the operator is a morphological opening working on the grayscale (Figure 3). The operations performed by the filter are erosion and dilation (Soille 2003). The first one consists in deleting every object smaller than the structuring element (here a disk with a radius of 2 pixels). The second is used to fill the gaps, between objects, that are smaller than the structuring element. These operations are followed by the removal of vegetal elements exploiting the high contrast between rock and vegetation in the red band of the orthophoto.

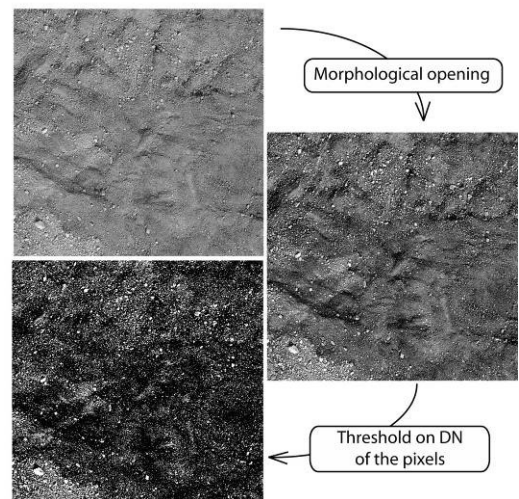


Figure 3. Remote sensing analysis on blocks' diameter.

Several analyses are conducted to study the morphology of the Frank slide deposit: flow network, roughness index and slope index. The first is based on a flow accumulation analysis. The second is an index of elevation variability performed with a neighbourhood analysis. Cavalli and Marci (2008) defined the roughness index as "the standard deviation of a residual topography". The third index is calculated using the same process, except that it is based on the slope. These

morphological analyses give indication of the granular flow type.

3 RESULTS

3.1 Folding

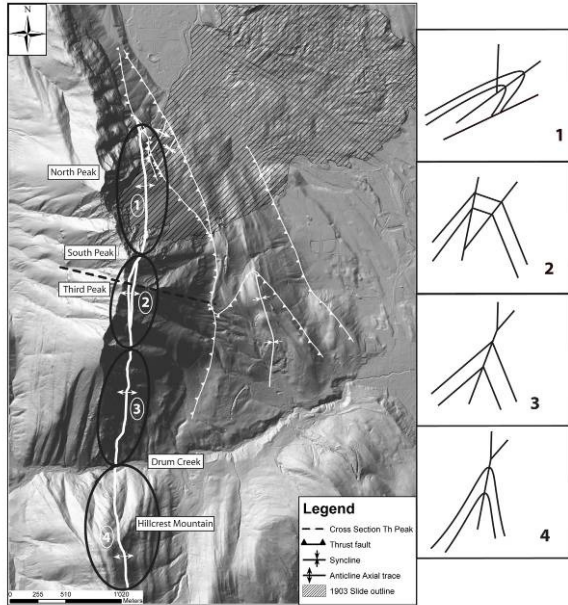


Figure 4. Turtle Mountain anticline's map with different hinge sectors. Sector 1's fold shape is more rounded than the others sectors.

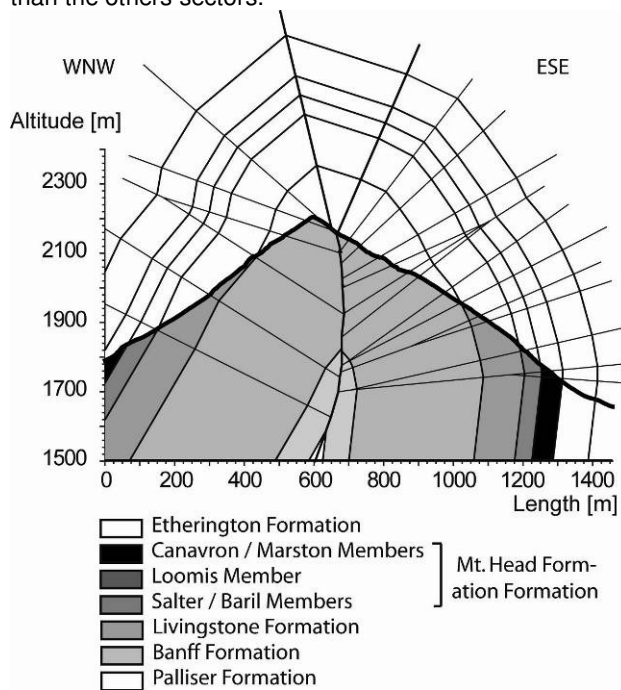


Figure 5. Turtle Mountain anticline's cross section with bold line indicating the hinge (686462/5494965 to 687881/5494624 NAD 1983 UTM 11N). See Figure 2 for stratigraphic informations.

The Turtle Mountain anticline was described as an asymmetric inclined fault propagation fold by Langenberg et al. (2007). This section is describing its geometry, especially of the hinge and the axial plunge.

The cross section presented in this study (Figure 5) described the fold as a chevron - box-fold type. The transition between the eastern and the western limbs happens in only few meters (5 to 10 m), especially in sectors 2 and 3 (Figure 4). The fold axis analysis, deduced from π diagram construction (Ramsay and Hubert 1987), shows that the axial culmination is situated near Third Peak. The fold axis plunges 2° towards 021° north of Third Peak, 5° to 22° towards 190° between Third Peak and Drum Creek and 20° towards 185° in Hillcrest Mountain.

Four propositions of fold geometry deduced from field work are presented in the following schemes (Figure 4). The axial surface is described as a slightly inclined simple hinge at depth which divides with height in two hinge segments in V shape at the top layers of the Livingstone formation. In sector 1, the anticline seems to be more inclined. The western segment of the hinge has here less influence in the anticline shape than in the other sectors of the fold.

3.2 Structure

The structural analysis on both limbs, based on more than 2000 samples data, permits to identify eight discontinuity sets. Bedding plane (BP), J1, J2, J3, J4 and J8 are almost present all over the investigated area, whereas two are more scattered (J5, J6). The results from Coltop 3D software are in good agreement with field survey analysis although J5 isn't detected because its orientation is very close to BP orientation. The nomenclature of discontinuity sets is consistent with Pedrazzini et al. (accepted), Jaboyedoff et al. (2009), Cruden and Krahn (1973) and Brideau et al. (in review), except J8 (which wasn't introduced before).

The area is split into homogenous fracturing zones in order to provide a total of 21 structural domains (SD) (Table 1).

Each SD shows approximately the same pattern of discontinuity sets with respect to the fold axis and the BP:

- Axial fracturing perpendicular to the BP (J3),
- Transverse sub-vertical fracturing (J8),
- Oblique fractures (J2 and J4),
- Sub-parallel to BP fracturing (J5),
- A $015^\circ/50^\circ \pm 20^\circ$ discontinuity set (J1),
- A $325^\circ/45^\circ \pm 20^\circ$ discontinuity set (J6).

The terminology characterizing the discontinuities is proposed by Ramsay and Huber (1987): axial (J3), transverse (J8) and oblique (J2 and J4).

Persistence, spacing, infilling, seepage, Joint Roughness Coefficient (using the Barton's comb), and large scale waviness measurements (ISRM 1977) were also carried out. In the hinge area, the persistence shows

higher values and the spacing lower values than elsewhere. For the others measurements, a clear trend is not observed.

Table 1. The 21 SD with corresponding mean values of discontinuity sets.

SD	BP	J1	J2	J3	J4	J5	J6	J8
1	259/54	012/61	050/33	161/41		232/38		153/77
2	261/64	022/32	055/36	121/44	166/64	242/54		357/64
3	275/41		046/65	099/46	164/59			018/90
4	288/51	022/67	053/67	118/50	187/63	271/78	319/60	193/89
5	288/44	017/60	069/59	127/50	184/65	289/49	318/56	185/81
6								
7	110/68	001/58	044/48	274/54	223/53	117/37	333/41	015/87
8	257/40	016/66	049/49	105/52	153/71			001/84
9		024/50						016/89
10	109/50	002/61		291/39	228/70			024/85
11	279/57	008/67	054/57	116/38	201/61	279/76	324/69	358/84
12	102/59	002/56				275/49		016/87
13	277/52	009/62	050/70	144/58	193/68	245/49	332/67	188/88
14	110/69	003/38		296/23	205/54			009/83
15	265/52	020/52	049/40	116/42	163/42			183/88
16	272/65	010/51	063/62	093/62		281/77	326/57	191/85
17	281/57	020/53	062/44	121/42		270/85		
18	095/78	359/46		262/22	185/48	094/34	326/47	180/78
19	274/79	009/51	055/45	146/37	165/75	270/73		
20		015/39		074/75				356/86
21	267/43	028/25	060/40	108/46	169/51	266/66	338/55	008/79

Back cracks mapping was performed on the orthophoto between North and Third Peaks. It shows a saw tooth trend. The strike direction is double: 0° - 180° and $135^{\circ} \pm 10^{\circ}$ - $315^{\circ} \pm 10^{\circ}$. Their gravitational movement direction corresponds to the orientation changes of the sets between SD 2 and 3. This change in orientation that symbolises the direction of the movement is estimated at $045^{\circ} / 15^{\circ} \pm 15^{\circ}$.

3.3 Rock mass condition

In order to provide a rock mass condition characterization, four measurements are conducted: UCS, IRS, Weathering Grade and GSI.

Both UCS and IRS give consistent results: IRS mainly ranges between R4 and R5 which corresponds to a UCS of 50 to 250 MPa. Direct measurements of UCS (using the L-type Schmidt hammer) display a trend between 100 and 150 MPa for a density of 2.55 to 2.6 gcm⁻³ (Figure 6). The abacus in ISRM 1977 was used to transform the number of Schmidt hammer rebounds in MPa. It is interesting to note that the measurements taken close to the hinge area present generally slightly lower values of UCS than elsewhere.

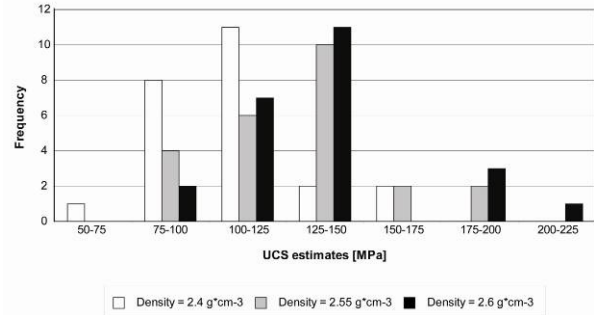


Figure 6. UCS frequency by density.

Weathering grade mean value corresponds to 2.5. It indicates a medium weathered rate in the anticline scale.

Considering the three above parameters, the Mount-Head formation's outcrops are generally in a better quality than those belonging to the Livingstone formation (IRS and UCS higher, Weathering grade lower) despite the fact that the spacing between discontinuities is generally lower (Pedrazzini et al. submitted).

The GSI estimates are presented in Figure 7. It shows a normal distribution with an average value from 35 to 50. These results correspond approximately to the studies of Pedrazzini et al. (accepted) and Brideau et al. (2010). The trend linking the GSI and the geological formations is not clear. Nevertheless, a trend is underlined considering lithologies. Indeed, fine-grained limestone shows slightly higher values than coarse-grained. Furthermore, some measurements are compared with the quantitative method proposed by Cai et al (2004) and show good accordance.

A relationship between the GSI and the structural domains is underlined. As expected, the SD located near the hinge present lower values of GSI than SD located in the limbs. Besides, a statistical model is applied to emphasize this relationship. In order to confirm that two distinct populations of data exist (measurement location < 70 m to the hinge and > 70m to the hinge), a Kolomogorov-Smirnov statistical test is carried out prior the SVR modeling. As expected, low values of GSI are found close to the hinge.

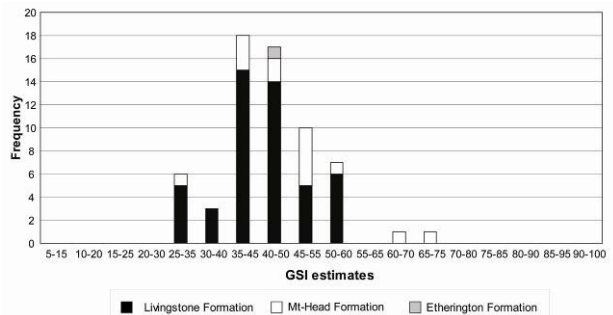


Figure 7. GSI estimates by geological formations.

Elsewhere, GSI values are higher and fluctuating as a consequence of other factors. Figure 8 is presenting the

spatial prediction of GSI from the distance to the hinge, the XY coordinates and the elevation. SVR's hyperparameters are optimized by 10-fold cross-validation. The model integrating these four patterns has lower errors and higher correlation between measured and predicted data on independent testing data on an independent testing subset compared to the model using only the distance. A visual interpretation of predictions confirms the ability of SVR to characterize the low values of GSI in the region of the hinge.

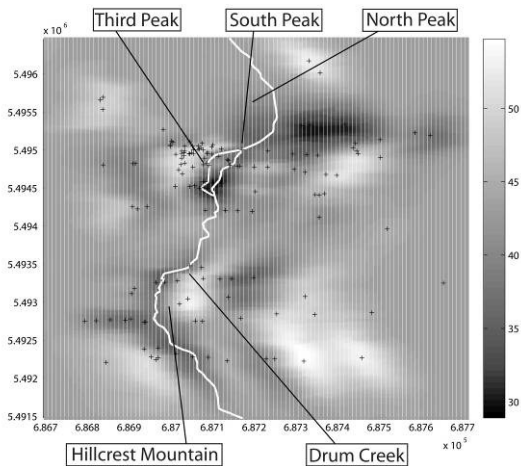


Figure 8. GSI's SVR spatial predictions from X,Y coordinates, elevation and the distance to the hinge (testing correlation ~ 0.57-0.63). Black crosses are the measurements.

3.4 Description of the deposit

3.4.1 Geological description

Based on field survey, a lithological analysis of the blocks was performed in order to underline the spatial distribution of the geological formations on the deposit. The Middle Livingstone, major component of the rock avalanche, is present everywhere on the surface of the deposit. The Upper Livingstone formation, initially compounding the top of the failed mass, is mainly observed in the proximal and central parts of the deposit. The Lower Livingstone formation as well as the Banff formation, are corresponding to the hinge area, are only found in the distal part of the deposit. The Palliser formation which was originally located in the heart of the anticline is not found on the deposit's surface.

3.4.2 Granulometrical description

Field work shows that the blocks are globally bigger in the central and in the eastern zones of the deposit. Besides, a relationship between the diameter and the distance to the scar is observed (Figure 9). This is underlined by the uniformity coefficient (C_u). It is defined as the ratio between D_{60} and D_{10} . Lower is its value, more uniform is the granulometric curve. So, the higher

C_u is, the higher the proportion of large blocks is. And, it is observed that the bigger blocks travelled further. The inflection of the polynomial curve corresponding to the far end of the deposit (Figure 9) can be interpreted as the "splash" area described by Cruden and Hungr (1986). It corresponds to the slide margins where big blocks are less observed and where vegetation is present emphasizing a higher proportion of fines.

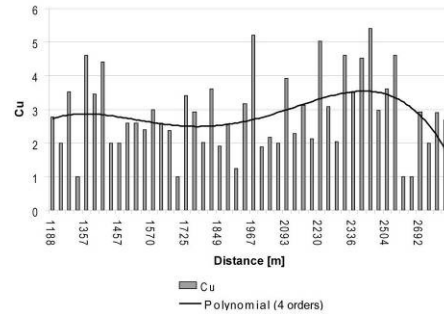


Figure 9. Uniformity coefficient depending of the distance to the scar.

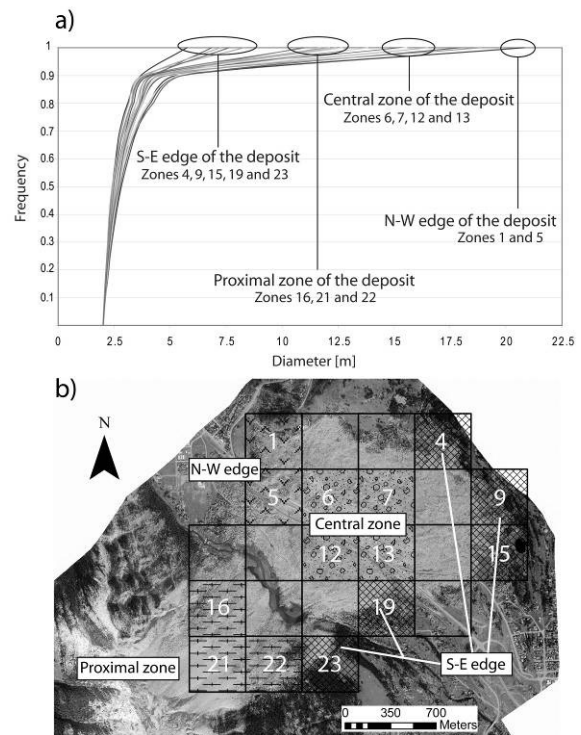


Figure 10. a) Granulometric curves obtained by remote sensing analysis showing homogeneous zones. b) Localisation of the zones of homogeneous granulometry.

Remote sensing analysis leads to a spatial distribution of the blocks on the entire deposit. Four homogeneous zones are identified (Figure 10). The S-E edge of the deposit presents the more homogenous granulometry with no block exceeding 9 m of diameter. Bigger blocks (never >13 m) are found in the proximal

zone of the deposit. The granulometry of the central zone is less uniform as blocks up to 16 m of diameter are measured. But the biggest blocks present in the deposit are found in the N-W edge of the deposit. In fact, the most massive blocks reach diameters of 20 m.

3.4.3 Morphological description

The flow accumulation analysis shows that the deposit can be separated into three zones (Figure 11). The first one, situated between the river and the road, presents a flow direction parallel to the direction of the propagation of the slide. This can be interpreted as an evidence of longitudinal ridges, features that are often seen on rock avalanches deposits (Dufresne, 2009). The second zone (eastern part of the deposit) shows the same characteristics. Inversely, the distal part presents a flow direction globally perpendicular to the propagation. The roughness and the slope indexes show the same features.



Figure 11. Flow accumulation analysis and ridges features.

4 DISCUSSION

4.1 Fold related and post folding fractures

The discontinuity sets can be linked with the tectonic phases described by Cooper (1992) and Price et al. (1986). Chronologically, these are:

- Folding and thrusting phase, direction E-W
- Transpression phase, direction NE-SW
- Extension phase, direction NW-SE

The field survey didn't point out any folded discontinuity indicating that none of them are anterior to the folding phase. Based on a smaller amount of data, this observation was already done (Pedrazzini et al. accepted). The same authors already suspected a syn-folding relationship for J2, J3 and J4. This hypothesis is verified and confirmed. On the seven discontinuity sets pointed out in this study (without the BP), four of them

(J2, J3, J4, J8) are considered as syn-folding regarding on geometrical parameters (Figure 12) and on the characteristics of the discontinuities. J3 and J8 are respectively axial and transverse fracturing with respect to the fold axis and generally appear perpendicular to BP. J3 ($110^{\circ}/45^{\circ} \pm 15^{\circ}$ in the western limb and $280^{\circ}/40^{\circ} \pm 15^{\circ}$ in the eastern limb) is probably a typical extension fracture considering its orientation and large calcite infilling. J8 ($000^{\circ}\text{-}180^{\circ}/86^{\circ} \pm 10^{\circ}$) is interpreted as an early fracture which is affected by shearing in the latest tectonic phase (extension and stress release). In fact, aside from the geometrical criterion, another argument confirms this hypothesis: Bazalgette (2004) propose to explain such a fracturing as a result of an early fracturing that grows with the folding amplification and that are reactivated in a shearing way if a fold axis parallel extension regime takes place. This explanation can likely be applied in this case. J2 ($050^{\circ}/50^{\circ} \pm 15^{\circ}$) and J4 ($170^{\circ}/55^{\circ} \pm 15^{\circ}$) are considered as strike slip conjugate discontinuities. Indeed, their orientations are consistent with the suspected major stress regime orientation occurring during the folding phase (W-E). Few evidences of shearing were observed on the field. Moreover, the low rock mass quality in outcrops didn't often allow the identification of the direction of shearing.

Based on the assumption that J2, J3, J4 and J8 are syn-folding, a reconstruction of the orientation of the paleo-stress regime during the folding phase is attempted. The construction method is defined by Kauffmann (2002). This is done for four structural domains of the western limb (Figure 13) and their results are coherent. J3 and J8 are not used for the construction but their respective orientations are in agreement with the stress directions.

Other fractures (J1, J5, and J6) have probably a post-folding origin and are linked with the transpressive phase. Back cracks follow J2 and J3. They are the expression of the extensional and stress release phase.

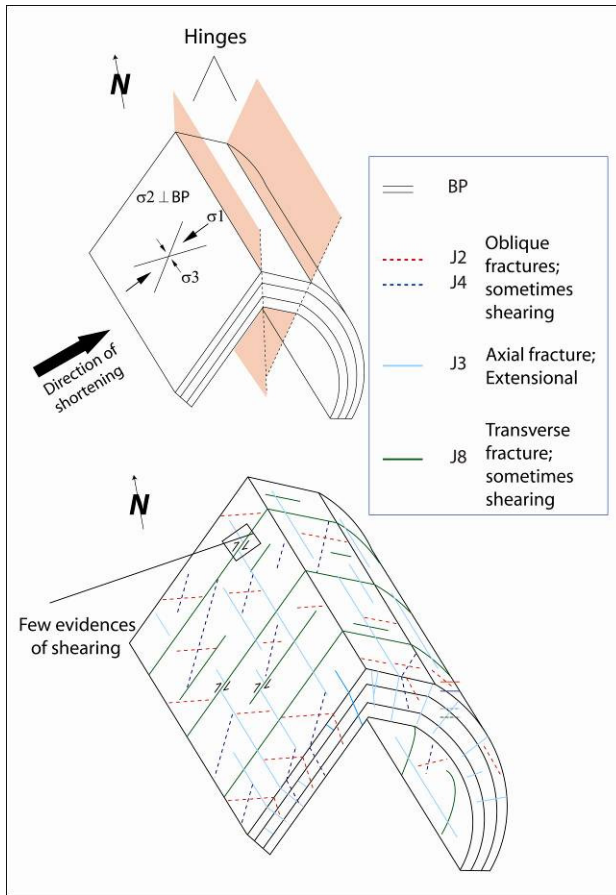


Figure 12. Scheme of the fold geometry. Positioning of fold related fractures and direction of major stresses.

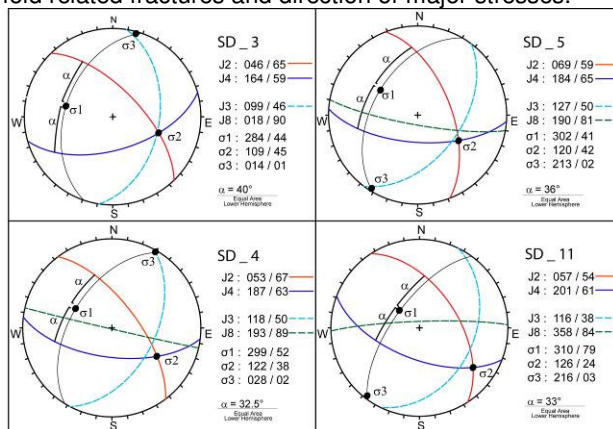


Figure 13. Major stress deduced from construction for SD 3, 4, 5 and 11.

4.2 Hinge influence on the rock mass quality

The hypothesis of the decrease of the GSI with the hinge distance is verified. The SD domains situated in the hinge area present lower values than those located in the limbs of the fold. This can be likely explained by a densification of the fracturing in the hinge. It was observed that the spacing between discontinuities (as the

block volume) decreases as the aperture between rock walls of the open discontinuities increases, especially for J3 (axial fracture). Consequently, the weathering grade slightly increases. The hinge of a fold is expected to be the zone that underwent the strongest strain resulting from traction, especially in the external part. Thus, in a brittle strain regime, as it is the case here, it is not surprising to assist to a higher fracturing in this area. Moreover, the grain size of the rocks influences the GSI. Furthermore, the SVR predictive model based on the field surveys measurements is able clearly to reproduce the relationship between the hinge and the GSI (Figure 8).

4.3 Description of the deposit

Based on the analysis of the geological formations on the deposit, a mode of collapse is proposed. The whole mass fragmented first and was affected by simple shearing. This progressively tilted the hinge area downwards until it was in a direction allowing the surface failure. Thus, the toe of the mountain fell down permitting the hinge's part to follow. As its energy was higher, its blocks travelled further. This is coherent with the fact that the hinge's geological formations are only observed at the distal part of the deposit. It was then permitted to the top of the mountain to collapse. As it succeeded to the toe and the hinge's part, it was curbed and it travelled a smaller distance. That is why, its compounding rocks (Upper Livingstone) are mainly found in the proximal part of the deposit.

The granulometrical analysis is coherent with this mode of collapse. The biggest blocks are observed in the central part and in the N-W edge. They formed probably the top of the mountain and were curbed by the first stage deposit.

The morphological analysis confirms the presence of longitudinal ridges on the deposit. This underlines some characteristics of the granular flow type: nonuniform grain size distribution and high-velocity flow (Dufresne, 2009). The presence of compressional ridges due to flow deceleration.

5 CONCLUSIONS

The structural study along with GSI modeling analyses verifies and completes the previous studies. Indeed, the relationship between fracturing and folding tectonic phase is confirmed by the reconstruction of the folding paleo-stress regime. It can be now assured that the failure of the 1903's event was structurally controlled. The GSI modelling corroborates the prior assumption that the rock mass condition depends mainly on the hinge position. The description of the deposit allows proposing a collapse mode. Moreover, it can help to understand the type of flow. Ridges and inverse grading distribution underline a granular flow process. This opens new perspectives for the modeling of this case's study.

ACKNOWLEDGEMENTS

The writers would like to acknowledge the contribution of Willem Langenberg and Marc-André Brideau for their assistance.

REFERENCES

- Bazalgette, L. 2004. *Relation plissement/fracturation multi-échelle dans les multicouches sédimentaires du domaine élastique/fragile : Accommodation discontinue de la courbure par la fracturation de petite échelle et par les articulations. Possibles implications dynamiques dans les écoulements des réservoirs*, Ph.D Thesis, University of Montpellier II, France.
- Benko, B., and Stead, D. 1998. The Frank slide: a reexamination of the failure mechanism, *Canadian Geotechnical Journal*, 35: 299-311.
- Brideau, M.A., Pedrazzini, A., Stead, D., Forese, C.R., Jaboyedoff, M., and Van Zeyl, D. Three dimensional slope stability analysis of South-Peak, Alberta, Canada. In review.
- Cai, M., Kaiser, P.K., Uno, H., Tasaka, Y., and Minami, M. 2004. Estimation of rock mass deformation modulus and strength of jointed hard rock masses using GSI system, *International Journal of Rock Mechanics & Mining Sciences*, 41: 3-19.
- Cavalli, M., and Marchi, L. 2008. Characterisation of the surface morphology of an alpine fan using airborne LiDAR, *Natural Hazards and Earth System Sciences*, 8: 323-333.
- Cooper, M. 1992. The analysis of fracture systems in subsurface thrust structures from the Foothills of the Canadian Rockies, in: *Thrust Tectonics*, edited by: McClay, K.R., Chapman and Hall, London.
- Couture, R., Locat, J., Drapeau, J.P., Evans, S.G., and Hadjigeorgiou, J. 1998. Evaluation de la granulométrie à la surface de débris d'avalanche rocheuse par l'analyse d'images, in: *Proceedings of the 8th International Congress of the International Association for Engineering Geology and the Environment, Vancouver, B.C.*, edited by: Moore, D.P., and Hungr, O., A.A. Balkema, Rotterdam, the Netherlands, 2:1383-1390.
- Couture, R., Locat, J., Hadjigeorgiou, J., Evans, S.G., and Antoine, P. 1996. Développement d'une technique de caractérisation des débris d'écroulements rocheux, in: *Proceedings of the 7th International Symposium on Landslides, Trondheim*, edited by: Senneset, A.A. Balkema, Rotterdam, the Netherlands, 1177-1182.
- Cruden, D.M., and Hungr, O. 1986. The debris of the Frank slide and theories of rockslide-avalanche mobility, *Canadian Journal of Earth Sciences*, 23, 425-432.
- Cruden, D.M., and Krahn, J. 1973. A re-examination of the geology of the Frank slide, *Canadian Geotechnical Journal*, 10, 581-591.
- Cruden, D.M., and Martin, C.D. 2007. Before the Frank slide, *Canadian Geotechnical Journal*, 44: 765-780.
- Dufresne, A. 2009. *Influence of runout path material on rock and debris avalanche mobility: field evidence and analogue modelling*, Ph.D Thesis, University of Canterbury, New Zealand.
- Froese, C., Jaboyedoff, M., Pedrazzini, A., Hungr, O., and Moreno, F. 2009a. Hazard mapping for the eastern face of Turtle Mountain, adjacent to the Frank slide, Alberta, Canada, in: *Proceedings of the Landslide Processes Conference, 6-7 February 2009, Strasbourg, France*.
- Froese, C., Moreno, F., Jaboyedoff, M., and Cruden, D.M. 2009b. 25 years of movement monitoring on the South Peak of Turtle Mountain: understanding the hazard, *Canadian Geotechnical Journal*, 46: 256-269.
- Groshong, R.H. 1999. *3D structural geology: a practical guide to surface and subsurface map interpretation*, Springer-Verlag, Berlin, Germany.
- Hoek, E., and Brown, E.T. 1997. Practical estimates of rock mass strength, *International Journal of Rock Mechanics & Mining Sciences*, 34: 1165-1186.
- International Society of Rock Mechanics (ISRM). 1977. Suggested methods for quantitative description of discontinuities in rock masses, *International Journal of Rock Mechanics & Mining Sciences & Geomechanics*, 15:319-358.
- Jaboyedoff, M., Couture, R., and Locat, P. 2009. Structural analysis of Turtle Mountain (Alberta) using digital elevation model: Toward a progressive failure, *Geomorphology*, 103: 5-16.
- Jaboyedoff, M., Metzger, R., Oppikofer, T., Couture, R., Derron, M.-D., Locat, J., and Turnel, D. 2007. New insight techniques to analyze rock slope relief using DEM and 3D-imaging cloud points: COLTOP-3D software, in: *Rock Mechanics: Meetings Society's Challenges and Demands*, edited by: Eberhardt, E., Stead, D. and Morrison, T., Taylor & Francis, 1: 61-68.
- Jones, P.B. 1993. Structural geology of the modern Frank slide and ancient Bluff Mountain slide, Crownest, Alberta, *Bulletin of Canadian Petroleum Geology*, 41: 232-243.
- Kauffmann, J.F. 2002. *Etude du tassement des Monts de Bex par géophysique et analyse de la fracturation*, Master Thesis, University of Lausanne, Switzerland.
- Langenberg, C.W., Pana, D., Richards, B.C., Spratt, D.A., and Lamb, M.A. 2007. Structural geology of the Turtle Mountain area near Frank, Alberta, *EUB/AGS Earth Sciences Report*, 2007-3.
- Locat, P., Couture, R., Leroueil, S., Locat, J., and Jaboyedoff, M. 2006. Fragmentation energy in rock avalanches, *Canadian Geotechnical Journal*, 43: 830-851.
- Marinos, V., Marinos, P., and Hoek, E. 2005. The geological strength index: applications and limitations, *Bulletin of Engineering Geology and the Environment*, 64: 55-65.
- McConnell, R.G., and Brock, R.W. 1903. *Report on the great landslide at Frank, Alberta*, Department of the Interior, Annual report for 1903, Ottawa, part 8, Edmonton Geological Society, 2003.

- Moreno, F., and Froese, C.R. 2007. Turtle Mountain field laboratory, monitoring and research summary report, January to December 2005, *Alberta Energy and Utilities Board, EUB/AGS Earth Sciences Report, 2006-7*.
- Norris, D.K. 1993. Geology and structure cross-sections, Blairmore (West half), Alberta, Geological Survey of Canada, Map 1829A, scale 1:50'000.
- Pedrazzini, A., Jaboyedoff, M., Froese, C.R., Langenberg, C.W., and Moreno, F. Accepted. Structural analysis of Turtle Mountain; origin and influence of fractures in the development of rock failure.
- Price, R.A., and Carmichael, D.M. 1986. Geometric test for Late Cretaceous-Paleogene intracontinental transform faulting in the Canadian Cordillera, *Geology*, 14: 468-471.
- Ramsay, J.G. and Huber, M.I. 1987. *The techniques of Modern Structural geology*, vol.2, Academic Press, London, England.
- Read, R.S., Savigny, K.W., Oboni, F., Cruden, D.M., and Langenberg, C.W. 2000. *Geotechnical hazard assessment of the south flank of Frank slide, Hillcrest, Alberta*, Geo Canada 2000, The Millenium Geoscience Summit, Calgary, Canada, May 29 – June 2 2000.
- Sturzenegger, M., Stead, D., Froese, C., Moreno, F., and Jaboyedoff, M. 2007. Ground based and airborne LiDAR for structural mapping of the Frank slide, in: *Proceedings of the 1st Canada-US rock mechanics Symposium, Vancouver, Canada, 27-31 May 2007*.
- Soille, P. 2003. *Morphological image analysis: Principles and applications*, 2nd ed., Springer-Verlag, Berlin, Germany.
- Vapnik, V.N. 1995. *The nature of statistical learning theory*, 2nd ed., Springer-Verlag, New York, USA.